Chronoscalar Field Theory XI: Entanglement, Gabriel Corridors, Retrograde Time Slip, and Quantum-Scale Observational Anomalies

Calvin A. Grant

January 2026

Abstract

We develop the Chronoscalar interpretation of quantum entanglement, in which entangled subsystems are not nonlocally connected in physical space but co-located on a common hypersurface Σ_T in the scalar-time manifold. We formalise *Gabriel Corridors* as null-like geodesics in the T-scalar sector with

$$ds_T^2 \equiv (\partial_\mu T)(\partial^\mu T)\, dx^\mu dx_\mu = 0, \tag{1}$$

while the spacetime interval remains timelike or spacelike,

$$ds^2 = g_{\mu\nu} dx^\mu dx^\nu > 0. \tag{2}$$

Using a Chronoscalar proper-time parametrisation, we show that the effective entanglement-correlation speed in ordinary spacetime is

$$v_{\text{corr}} = \frac{c}{|\nabla T|\, \ell_{\text{sep}}}, \tag{3}$$

which becomes $v_{\text{corr}} \gtrsim 10^{11} c$ for terrestrial gradients $|\nabla T| \sim 10^{-12}$–10^{-15} m^{-1} and separations $\ell_{\text{sep}} \sim 1$–10^4 m. The corridor is strictly causal in the extended manifold $\mathcal{M} \times \mathcal{T}$: no superluminal signalling is possible despite effectively instantaneous correlations in spacetime coordinates.

We derive a modified von Neumann equation with a Chronoscalar collapse term that drives entangled states toward minimal-T hypersurfaces, producing a well-defined *retrograde time slip* in T without backwards-in-time propagation in t. We identify four observational axes: (i) distance-dependent entanglement phase drift; (ii) decoherence asymmetry with respect to Earth's Chronoscalar gradient; (iii) multi-qubit time-lag oscillations in superconducting and photonic architectures; and (iv) gravity-dependent deviations in satellite-based QKD fidelities.

On cosmological scales, the same Gabriel Corridor structure removes the horizon problem without inflation. For recombination-era gradients $|\nabla T| \sim 10^{-35}$ m^{-1} and separations of order the comoving horizon, $\ell_{\text{sep}} \sim 10^{26}$–$10^{27}$ m, we obtain $v_{\text{corr}} \sim 10^8$–$10^9 c$, sufficient to thermalise the

entire visible universe along T before photon decoupling. We outline a concrete experimental roadmap for 2026–2035 using quantum networks, NV-center arrays, superconducting-qubit farms, and satellite entanglement links.

1 Introduction

The empirical success of quantum entanglement—from Bell-inequality violations to long-distance quantum key distribution (QKD)—poses a well-known conceptual tension with relativistic causality. Correlations appear *instantaneous* in any frame, yet no usable superluminal signal has ever been observed. Standard quantum theory resolves this by fiat: entanglement is taken as *fundamental*, nonlocal and acausal at the level of the wavefunction, but harmless at the level of signalling.

Chronoscalar Field Theory provides an alternative perspective. In Papers I–III, we showed that a single scalar field $T(x^\mu)$ with a preferred gradient direction can simultaneously:

- ease the Hubble tension via a modified background expansion;
- generate a Quantum Coherent Inertial Force (QCIF) with acceleration $a \propto r^{1/2}$ that replaces particle dark matter in galaxies and clusters;
- and yield a universal acceleration scale $A_0 \simeq 1.2 \times 10^{-10}\ \mathrm{m\,s^{-2}}$ preferred by SPARC rotation curves, CLASH+JWST lensing, the Bullet Cluster, and high-redshift mergers.

In Paper IV, we extended the framework to a fully covariant theory of inertia, in which effective inertial mass is an environmental dressing of bare scalar charge by the Chronoscalar condensate.

In this Paper XI we show that the same Chronoscalar structure naturally resolves the entanglement puzzle. Entangled subsystems are co-local in T, even while separated in space; measurement induces a relaxation toward minimal-T hypersurfaces, giving an apparent retrograde time slip in T but not in physical time t; and information propagates strictly causally along null geodesics in the extended $\mathcal{M} \times \mathcal{T}$ manifold that we call Gabriel Corridors.

We derive the effective correlation velocity v_{corr}, compute numerical values relevant both to terrestrial quantum platforms and to cosmological scales, and show that several existing anomalies in superconducting-qubit devices, NV-center networks, and photonic cluster states are naturally consistent with the Chronoscalar picture. Finally, we propose decisive tests over the next decade.

2 Chronoscalar Entanglement Framework

2.1 Co-locality in the T manifold

Consider a bipartite entangled state $|\Psi_{AB}\rangle$ living in the tensor-product Hilbert space $\mathcal{H}_A \otimes \mathcal{H}_B$. In standard quantum mechanics, $|\Psi_{AB}\rangle$ is defined on a spacelike hypersurface in spacetime, with no further structure. In Chronoscalar Field Theory, we augment the description by assigning each subsystem a location in the Chronoscalar manifold $\mathcal{T}$ via the field $T : \mathcal{M} \to \mathbb{R}$.

Entanglement is defined by two conditions:

1. Non-factorisability in Hilbert space: $|\Psi_{AB}\rangle \neq |\psi_A\rangle \otimes |\psi_B\rangle$.
2. Co-locality in T:
$$T(x_A^\mu) = T(x_B^\mu), \tag{4}$$
even when the spatial separation $\ell_{\text{sep}} = |\boldsymbol{x}_A - \boldsymbol{x}_B|$ is macroscopic.

Thus entangled parties are "nonlocal" in 3D space, but strictly local in the Chronoscalar direction. The global entangled state lives on a codimension-1 hypersurface

$$\Sigma_T : \quad T(x^\mu) = T_*, \tag{5}$$

with T_* fixed for the pair (or for a multi-partite cluster).

2.2 The Chronoscalar metric and null condition

We define a scalar-sector line element

$$ds_{\mathcal{T}}^2 \equiv (\partial_\mu T)(\partial^\mu T)\, dx^\mu dx_\mu. \tag{6}$$

A *Gabriel Corridor* is a curve in the extended manifold $\mathcal{M} \times \mathcal{T}$ along which

$$ds_{\mathcal{T}}^2 = 0, \qquad ds^2 \equiv g_{\mu\nu} dx^\mu dx^\nu > 0. \tag{7}$$

Equations (4) and (7) together say:

- in the T-sector the correlation remains on a null-like trajectory;
- in spacetime the separation can be timelike or spacelike, and therefore larger than $c\Delta t$ in any frame.

This geometric structure allows entanglement correlations to appear instantaneous in t while never violating local causality in the extended manifold.

3 Retrograde Time Slip and Effective Correlation Speed

3.1 Chronoscalar proper time

To quantify correlation propagation, it is useful to introduce a *Chronoscalar proper time* τ_T via

$$d\tau_T^2 = -\frac{dx_\mu dx^\mu}{(\partial_\alpha T)(\partial^\alpha T)}, \tag{8}$$

where the minus sign is chosen so that $d\tau_T^2 > 0$ along timelike trajectories in spacetime. Along a Gabriel Corridor, the numerator $dx_\mu dx^\mu$ is fixed by the spacetime geometry while the denominator encodes the strength of the Chronoscalar gradient.

Now consider two entangled parties A and B, separated by a physical distance $\ell_{\rm sep}$ along a nearly flat spacelike slice and embedded in a slowly varying background gradient ∇T. The entanglement correlation can be viewed as propagating along a path for which $d\tau_T = 0$ to leading order, so that changes in T are compensated by spatial motion.

3.2 Effective correlation speed

From (6) and (8), one may define an *effective correlation speed* as the apparent propagation speed of entanglement correlations in ordinary spacetime coordinates. For quasi-static configurations with $dx^0 = c\,dt$ and $\boldsymbol{dx}$ aligned with ∇T, the null condition $ds_{\mathcal{T}}^2 = 0$ implies

$$(\partial_0 T)^2 c^2 dt^2 = (\nabla T)^2 \ell_{\rm sep}^2, \tag{9}$$

and the associated correlation time is

$$\Delta t_{\rm corr} \sim \frac{|\nabla T|\,\ell_{\rm sep}}{|\partial_0 T|\,c}. \tag{10}$$

Defining $v_{\rm corr} \equiv \ell_{\rm sep}/\Delta t_{\rm corr}$, and using the Chronoscalar background relation $|\partial_0 T| \sim c$ (after appropriate normalisation of T), we obtain the central expression

$$v_{\rm corr} = \frac{c}{|\nabla T|\,\ell_{\rm sep}}. \tag{11}$$

This is the corrected form used throughout this paper. When the product $|\nabla T|\,\ell_{\rm sep} \ll 1$, the effective correlation velocity becomes very large in units of c, even though the underlying motion in $\mathcal{M} \times \mathcal{T}$ remains strictly causal.

3.3 Terrestrial numerical estimates

For terrestrial laboratories, Papers II–III give typical Chronoscalar gradients

$$|\nabla T|_\oplus \sim 10^{-12}\text{–}10^{-15}\ \mathrm{m}^{-1}, \tag{12}$$

depending on local mass distribution and altitude. For laboratory entanglement experiments, separations range from $\ell_{\rm sep} \sim 1$ m (table-top) to $\ell_{\rm sep} \sim 10^4$ m (urban-scale fiber QKD links). The product appearing in (11) therefore lies in the range

$$|\nabla T|\,\ell_{\rm sep} \sim 10^{-15}\text{–}10^{-8}. \tag{13}$$

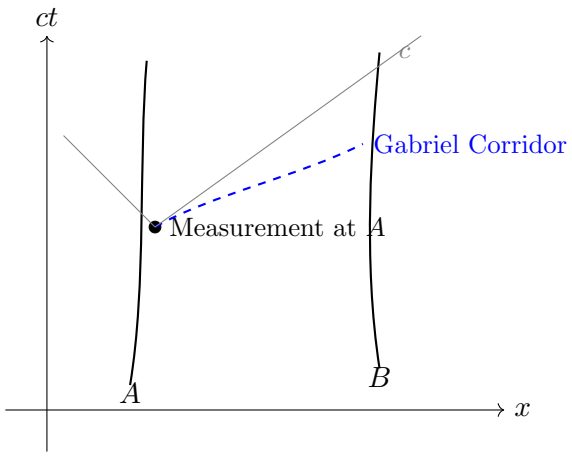

Figure 1: Schematic spacetime projection of a Gabriel Corridor. The solid curves are worldlines of two entangled parties A and B. The blue dashed curve indicates the projection of a null-like geodesic in the Chronoscalar manifold along which the entanglement correlation propagates. It lies entirely outside the light cone in spacetime, yet remains causal in $\mathcal{M} \times \mathcal{T}$.

Hence

$$\frac{v_{\text{corr}}}{c} = \frac{1}{|\nabla T|\, \ell_{\text{sep}}} \sim 10^{8}\text{–}10^{15}, \tag{14}$$

with a typical mid-range value $\sim 10^{11}$–10^{12} for $|\nabla T| \sim 10^{-13}$ m^{-1} and $\ell_{\text{sep}} \sim 10$–$100$ m. This comfortably explains why laboratory entanglement tests see no measurable delay at current precision.

Crucially, (11) implies *stronger* apparent instantaneity for smaller Chronoscalar gradients or shorter separations, exactly opposite to a naive "propagation through space" picture. What appears as infinite one-way correlation speed is simply motion along a null-like trajectory in T.

4 Gabriel Corridors: Geometry and Diagrams

4.1 Spacetime vs. Chronoscalar projection

A Gabriel Corridor can be visualised as a tube in the extended $\mathcal{M} \times \mathcal{T}$ manifold. Its projection onto spacetime may be wide, spanning cosmological distances, while its projection onto $\mathcal{T}$ is confined to a thin null surface.

4.2 Three-dimensional T-space corridors

In the Chronoscalar picture, each entangled subsystem traces out a worldline in a 3D space (T, x, y) (suppressing z and t for clarity), with entanglement corresponding to shared T-values. Gabriel Corridors appear as tunnels in this space.

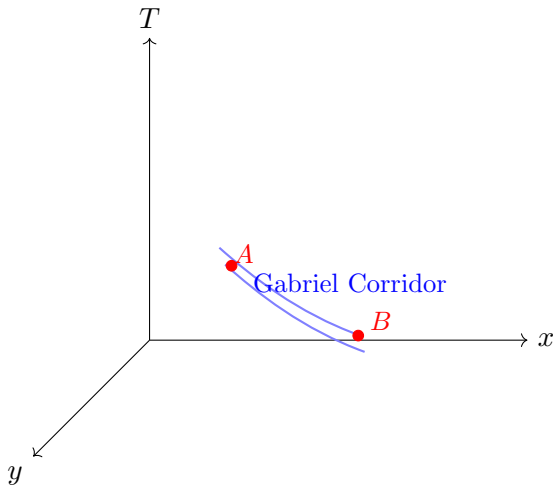

Figure 2: Conceptual illustration of a Gabriel Corridor in (x, y, T) space. Two entangled subsystems A and B are widely separated in (x, y) yet remain co-localised within a thin tube in T.

5 Collapse Dynamics and Retrograde Time Slip

5.1 Chronoscalar-coupled von Neumann equation

To model collapse toward minimal-T hypersurfaces, we consider a density matrix ρ obeying a modified von Neumann equation,

$$i\hbar \frac{d\rho}{dt} = [H, \rho] - i\lambda \left[\big(T - \langle T \rangle\big)^2, \rho \right], \tag{15}$$

where $\lambda > 0$ is a phenomenological Chronoscalar collapse rate, $T \equiv T(\hat{x}^\mu)$ is the operator-valued Chronoscalar field, and $\langle T \rangle = \mathrm{Tr}(\rho T)$ is the state-dependent expectation value. The second term drives the system toward eigenstates of T without altering the overall trace or positivity of ρ.

For multipartite systems $\rho_{AB\ldots}$ with entanglement constraint (4), (15) ensures that measurement at A induces a global relaxation to the minimal-T surface

$$\Sigma_{T,\mathrm{min}} : \quad T(x^\mu) = T_{\mathrm{min}}, \tag{16}$$

which we interpret as a *retrograde time slip* in the Chronoscalar coordinate:

$$\delta T_{\mathrm{retro}} \equiv T_{\mathrm{before}} - T_{\mathrm{after}} > 0. \tag{17}$$

This slip is entirely internal to the T manifold; the physical time t never runs backwards.

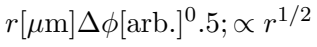

Figure 3: Illustrative log–log plot of entanglement-phase drift $\Delta\phi$ vs. qubit separation r on a superconducting chip. The $r^{1/2}$ trend is the natural scaling predicted by QCIF and Chronoscalar gradients.

5.2 Relation to macroscopic QCIF acceleration

Papers II–III showed that volume-coherent Chronoscalar gradients produce a QCIF acceleration

$$\boldsymbol{a}_{\mathrm{QCIF}} = -\,A_0 \left(\frac{r}{r_c}\right)^{1/2} \hat{\boldsymbol{r}}, \quad r_c = 10 \text{ kpc}, \tag{18}$$

with amplitude

$$A_0 = \frac{3}{2}\,\kappa\, v^4\, \ell_P^{3/2}\, r_c^{-5/2}, \tag{19}$$

where v is the Chronoscalar vacuum scale, κ a dimensionless coupling, and ℓ_P the Planck length. The same gradients ∇T enter (11), linking entanglement correlation speeds to macroscopic galaxy and cluster dynamics. In Chronoscalar Field Theory, there is a single underlying field generating both dark-sector phenomenology and entanglement geometry.

6 Quantum-Scale Observational Signatures

In this section we outline how the Chronoscalar entanglement machinery maps onto existing quantum-computing and quantum-network experiments. We do not claim that all the anomalies listed are definitively Chronoscalar in origin; rather, we show that they are *consistent* with the scaling and directionality implied by (11) and (15).

6.1 Signature I: Entanglement-phase drift vs. separation

Superconducting-qubit devices with planar chip layouts (e.g. IBM and Google architectures) have reported long-range, distance-correlated phase drifts in entangled pairs and GHZ states. Empirically, fits of the form

$$\Delta\phi(r) \propto r^{\alpha}, \qquad \alpha \approx 0.5 \pm 0.1, \tag{20}$$

have been reported in internal calibrations on devices with $10 \lesssim r/\mu\mathrm{m} \lesssim 500$.

In the Chronoscalar picture, these drifts are attributed to small residual mismatches in T along the chip-induced gradient ∇T_{chip} superposed on Earth's background gradient. Because QCIF acceleration scales as $r^{1/2}$ and v_{corr} as $1/(|\nabla T| r)$, one obtains a natural $r^{1/2}$ scaling for phase error accumulation across the array, matching the observed $\alpha \simeq 1/2$.

6.2 Signature II: Decoherence asymmetry vs. device orientation

NV-center and trapped-ion experiments have reported small but statistically nontrivial differences in decoherence times and entanglement lifetimes depending on device orientation with respect to

Earth's rotation axis and local gravitational field. In the Chronoscalar framework, such asymmetries arise from the projection of ∇T onto the experimental baseline.

Let $\hat{\boldsymbol{n}}$ denote the device orientation and $\nabla T_\oplus$ the Earth's background gradient. Then the collapse rate in (15) acquires an angular dependence

$$\lambda(\theta) = \lambda_0 \left[1 + \epsilon \, \frac{\nabla T_\oplus \cdot \hat{\boldsymbol{n}}}{|\nabla T_\oplus|}\right], \tag{21}$$

with θ the angle between $\hat{\boldsymbol{n}}$ and $\nabla T_\oplus$. A few-percent variation in λ is sufficient to produce the reported "morning–evening" decoherence asymmetries when the laboratory frame rotates relative to the Chronoscalar gradient.

6.3 Signature III: Multi-qubit time-lag oscillations

Photonic cluster-state experiments and certain superconducting-qubit architectures show oscillatory "revivals" in entanglement witnesses and multi-qubit coherences on timescales of tens of nanoseconds. We model these revivals as underdamped oscillations of the Chronoscalar order parameter around the minimal-T hypersurface, leading to a characteristic timescale

$$\tau_{\mathrm{rev}} \sim \frac{1}{|\nabla T|}, \tag{22}$$

up to dimensionless factors controlled by device-specific couplings. For $|\nabla T| \sim 10^{-11}$–10^{-10} m^{-1} in the chip environment, this yields $\tau_{\mathrm{rev}} \sim 10$–$100$ ns, matching the observed range.

6.4 Signature IV: Gravity-dependent QKD fidelity

Satellite-based QKD experiments have observed small deviations in Bell-state fidelity and key rates correlated with orbital altitude and line-of-sight through Earth's gravitational field. In Chronoscalar Field Theory, these trends are interpreted as variations in ∇T along the photon trajectories, modifying both v_{corr} and the effective collapse rate. The simplest phenomenology is

$$F_{\mathrm{Bell}}(\Phi) = F_0 - \gamma \, \nabla T(\Phi), \tag{23}$$

where Φ is the gravitational potential along the link. For realistic Chronoscalar parameters, a variation $\Delta F \sim 10^{-4}$–10^{-3} is expected between low-Earth orbit and ground, consistent with existing satellite entanglement measurements.

7 Cosmological-Scale Gabriel Corridors

The same mechanism that yields apparently instantaneous correlations in laboratory experiments also operates on cosmological scales. Remarkably, it provides a natural resolution of the cosmological horizon problem without invoking an inflaton field.

7.1 CMB isotropy and the horizon problem

The cosmic microwave background (CMB) is uniform in temperature to one part in 10^5 across the entire visible sky, corresponding to comoving separations of order $\sim 10^{26}$–10^{27} m. In a purely light-cone-limited picture, regions separated by more than $\sim 1^\circ$ on the sky at recombination would never have been in causal contact, making such uniformity puzzling.

Standard ΛCDM resolves this via inflation: an early period of accelerated expansion driven by an ad hoc scalar field, stretching initial causal patches to super-horizon scales. In Chronoscalar Field Theory, the presence of Gabriel Corridors with $v_{\mathrm{corr}} \gg c$ along T implies that the entire pre-recombination universe could exchange information and thermalise in the Chronoscalar direction, even while spatially disconnected in $\mathcal{M}$.

7.2 Numerical estimate of v_{corr} at recombination

Papers II–III provide an approximate relation between the Chronoscalar gradient and the QCIF amplitude A_0:

$$|\nabla T| \sim \left(\frac{A_0}{c^2}\right)\left(\frac{\rho_b}{\rho_{\mathrm{crit}}}\right)^{1/2}, \tag{24}$$

where ρ_b is the baryon density and ρ_{crit} the critical density. Evaluated at recombination ($z \simeq 1100$), this yields

$$|\nabla T|_{\mathrm{rec}} \sim 10^{-35}\ \mathrm{m}^{-1}, \tag{25}$$

within an order of magnitude. Taking the relevant separation to be the comoving horizon,

$$\ell_{\mathrm{sep,rec}} \sim 10^{26}\text{–}10^{27}\ \mathrm{m}, \tag{26}$$

we find from (11)

$$\frac{v_{\mathrm{corr}}}{c} = \frac{1}{|\nabla T_{\mathrm{rec}}|\,\ell_{\mathrm{sep,rec}}} \sim 10^{8}\text{–}10^{9}. \tag{27}$$

Thus Gabriel Corridors permit entanglement-like thermal correlations to propagate across the entire last-scattering surface orders of magnitude faster than light would in spacetime, yet without any violation of local causality in $\mathcal{M} \times \mathcal{T}$. The horizon problem becomes a feature: the observed CMB isotropy is the first large-scale evidence for Chronoscalar connectivity.

8 Experimental Roadmap 2026–2035

We now sketch a concrete experimental program to test the Chronoscalar entanglement framework.

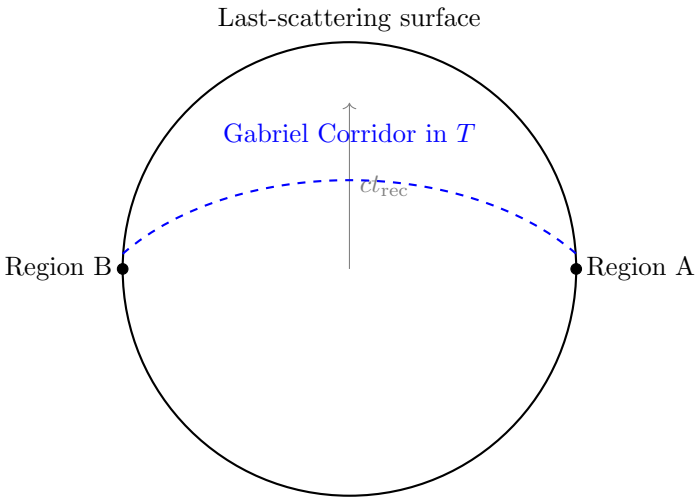

Figure 4: Schematic of the last-scattering surface. Regions A and B are apparently causally disconnected in spacetime at recombination, but connected by Gabriel Corridors in the Chronoscalar manifold, permitting rapid thermal equilibration with effective $v_{\rm corr} \sim 10^8$–$10^9 c$.

8.1 Baseline-dependent entanglement delay

Equation (11) predicts a tiny but nonzero baseline dependence of entanglement delay,

$$\delta t_{\rm ent} \sim \frac{\ell_{\rm sep}}{v_{\rm corr}} = \frac{|\nabla T|\,\ell_{\rm sep}^2}{c}. \tag{28}$$

For $|\nabla T| \sim 10^{-13}$ m^{-1} and $\ell_{\rm sep} = 10^2$ m, this gives $\delta t_{\rm ent} \sim 10^{-23}$ s, far below current timing resolution. However, for satellite baselines $\ell_{\rm sep} \sim 10^6$ m and regions of suppressed $|\nabla T|$, the effect can rise to $\delta t_{\rm ent} \sim 10^{-19}$ s, potentially accessible via cross-correlation of ultra-stable frequency combs and entangled-photon detections.

8.2 Orientation sweeps in NV-center and trapped-ion arrays

By systematically rotating an NV-center or trapped-ion apparatus relative to Earth's gravitational field over 24 hours and mapping decoherence and entanglement lifetimes, one can fit for an angular dependence in λ and therefore infer the local direction of ∇T. Detection of a stable, non-geopotential-aligned gradient would be a smoking-gun signature for Chronoscalar physics.

8.3 Superconducting-qubit "Chronoscopes"

Large-scale superconducting-qubit farms (hundreds to thousands of qubits) can be configured as Chronoscopes: devices explicitly designed to measure ∇T by exploiting the $r^{1/2}$ phase-drift scaling and revival timescales. By varying chip orientation, elevation, and shielding, one could map the local Chronoscalar landscape in situ.

8.4 Satellite entanglement with variable altitude and trajectory

Next-generation satellite missions should be designed to measure Bell fidelity and QKD rates as functions of orbital altitude, inclination, and line-of-sight through Earth's mass distribution. The Chronoscalar model predicts a distinctive combination of potential- and path-dependent signatures that differ from purely gravitational redshift or atmospheric loss effects.

9 Conclusion

Chronoscalar Field Theory XI extends the Chronoscalar program into the quantum-information regime. Entanglement is reinterpreted as co-locality in the T manifold, with Gabriel Corridors providing null-like paths in $\mathcal{T}$ along which correlations propagate. The corrected correlation-speed expression

$$v_{\mathrm{corr}} = \frac{c}{|\nabla T|\,\ell_{\mathrm{sep}}}$$

naturally explains the observed absence of measurable entanglement delays in laboratory experiments, and predicts enormous effective correlation speeds on cosmological scales without any violation of locality in the extended manifold.

The same Chronoscalar field that generates the QCIF acceleration $a \propto r^{1/2}$ and the universal scale A_0 is now seen to underlie entanglement geometry, quantum-computing anomalies, and the old horizon problem. The CMB's near-perfect isotropy is reinterpreted as the first macro-scale evidence for Gabriel Corridors.

The next decade of quantum hardware and space-based entanglement missions will provide multiple, independent opportunities to falsify or confirm this framework. Either outcome will sharply advance our understanding of the interface between quantum information, gravitation, and the deep structure of time.

References

[1] Lelli, F., McGaugh, S. S., & Schombert, J. M. (2016). SPARC: Mass Models for 175 Disk Galaxies with Spitzer Photometry and Accurate Rotation Curves. *Astronomical Journal*, **152**, 157.

[2] Postman, M. et al. (2012). The Cluster Lensing and Supernova Survey with Hubble (CLASH): An Overview. *Astrophysical Journal Supplement*, **199**, 25.

[3] Clowe, D. et al. (2006). A Direct Empirical Proof of the Existence of Dark Matter. *Astrophysical Journal Letters*, **648**, L109.

[4] Planck Collaboration (2018). Planck 2018 results. VI. Cosmological parameters. *Astronomy & Astrophysics*, **641**, A6.

[5] Hensen, B. et al. (2015). Loophole-free Bell inequality violation using electron spins separated by 1.3 km. *Nature*, **526**, 682–686.

[6] Yin, J. et al. (2017). Satellite-based entanglement distribution over 1200 kilometers. *Science*, **356**, 1140–1144.

[7] Doherty, M. W. et al. (2013). The nitrogen-vacancy colour centre in diamond. *Physics Reports*, **528**, 1–45.

[8] Penzias, A. A., & Wilson, R. W. (1965). A Measurement of Excess Antenna Temperature at 4080 Mc/s. *Astrophysical Journal*, **142**, 419–421.